Planet. Space Sci., Vol. 34, No. 11, pp. 1031–1035, 1986
Printed in Great Britain

0032-0633/86 $3.00+0.00

THE DAYGLOW OF THE O_2 ATMOSPHERIC BAND SYSTEM

A. BUCHOLTZ, W. R. SKINNER, V. J. ABREU and P. B. HAYS
Department of Atmospheric and Oceanic Science, Space Physics Research Laboratory, University of Michigan, Ann Arbor, MI 48109, U.S.A.

(*Received* 19 *May* 1986)

Abstract—The dayglow of the O_2 atmospheric band system has been simulated by taking into account the three main production mechanisms of the $O_2(^1\Sigma)$ state: resonance fluorescence, a photochemical term due to quenching of $O(^1D)$, and a pure chemical process. Values of the g factor, which are involved in the resonant scattering of the O_2 atmospheric bands (A, B and γ), have been obtained as a function of altitude (0–120 km) and solar zenith angle using a line-by-line calculation. The values of the g factor, along with updated rate coefficients, have been used in the calculation of the production rate of $O_2(^1\Sigma)$ and the volume emission rate of the $(O_2\ ^1\Sigma, v'=0)$–$(O_2\ ^3\Sigma, v''=0)$ transition. The results of these calculations are compared to observational measurements and are found to be in excellent agreement.

1. INTRODUCTION

Wallace and Hunten (1968) studied the dayglow O_2 atmospheric band system in detail. Carrying out a series of rocket observations using spectrometers and photometers in the altitude range 35–128 km, they identified the main production mechanisms of the $O_2(^1\Sigma)$ states: quenching of $O(^1D)$ from 90 km to the lower thermosphere, resonance scattering in the 70–90 km region, and photolysis of ozone in the 35–70 km region. The latter was thought to consist of two processes: the direct photolysis of ozone, and an indirect channel in which ozone is photolysed to produce $O(^1D)$ which is in turn quenched by O_2. Later work, however, has shown the direct photolysis of ozone to be ineffective (Gauthier and Snelling, 1970, 1971). Wallace and Hunten also postulated a small chemical source near 90 km to account for an excess of emission at that altitude which could not be accounted for by resonance scattering and energy transfer from $O(^1D)$. They suggested a Chapman type reaction but later studies have favored the Barth mechanism (Campell and Gray, 1973; Greer *et al.*, 1981; Slanger and Black, 1977).

The Space Physics Research Laboratory is currently working on the development of the High Resolution Doppler Imager (HRDI) which is a triple etalon Fabry–Perot Interferometer to be flown on the Upper Atmosphere Research Satellite (UARS). This instrument will measure temperatures and winds in the middle atmosphere by looking at emission and absorption lines in the O_2 atmospheric band system, $b\ ^1\Sigma_g^+ - X\ ^3\Sigma_g^-$. Accurate simulations of this band system in absorption and emission are required for instrument development and data interpretation at a later stage. Our model builds on the work of Wallace and Hunten by employing improved density profiles for ozone and atomic oxygen (S. Solomon, private communication), taking into account the Barth mechanism near 90 km, using updated rate coefficients for the different reactions and calculating more rigorously the emission rate or g factor due to resonance scattering. Wallace and Hunten, in their computation of the g factor, employed an average transmission function over the rotational structure of the band and assumed a Doppler line profile throughout the altitude range (35–128 km). The g factor is obtained here by using a line-by-line calculation which takes into account both the pressure broadening and the overlapping of lines in the spectrum. The consideration of pressure broadening effects allows us to extend the g factor calculation to lower altitudes.

This paper will discuss the production and loss processes of the $O_2(^1\Sigma)$ state employed in our model. First, we will explain our calculation of the emission rate factor. We will show how it varies from band to band and the effect solar zenith angle and pressure broadening have on its value. Next, we will discuss the chemical production mechanisms of $O_2(^1\Sigma)$ that we consider in the model, followed by a discussion of the loss processes involved. Finally, the production and volume emission rates obtained will be compared to the observational results of Wallace and Hunten (1968).

2. $O_2(^1\Sigma)$ PRODUCTION AND LOSS MECHANISMS

2.1. g-*Factor calculation*

The production rate of $O_2(b\,^1\Sigma_g^+)$ due to resonance scattering in the atmospheric bands as a function of altitude can be written as:

$$P_{RES}[O_2(^1\Sigma)] = n_{O_2}(z)\int_\nu \pi F(\nu, z)\sum_j S_J(T)V(T, P, x, y)\,d\nu \quad (1)$$

where z = altitude, $\pi F(\nu, z)$ = solar flux at wavenumber ν, $n_{O_2}(z) = O_2$ density at z, $S_J(T)$ = line strength of Jth line at temperature T, $V(T, P, x, y)$ = line shape at temperature T, pressure P, $x = (\nu - \nu_0)/\Delta\nu_D$, $y = \Delta\nu_L/\Delta\nu_D$, $\Delta\nu_D$ = Doppler half-width and $\Delta\nu_L$ = Lorentz half-width.

A Voigt profile, $V(T, P, x, y)$, was used in our model to represent the line shape, where x is the normalized distance from line center and y is the damping parameter (Drayson, 1976).

Equation (1) can also be written as

$$P_{RES}[O_2(^1\Sigma)] = n_{O_2}(z)g(z), \quad (2)$$

where $g(z)$ is defined as the emission rate factor and is equal to the integral in equation (1).

Since the solar flux is absorbed as it passes through the atmosphere its attenuation must be considered. At any altitude and wavenumber the solar flux, considering only O_2 absorption, is given by

$$\pi F(\nu, z) = \pi F(\nu, \infty)\exp[-\tau(\nu, z)], \quad (3)$$

where $\pi F[\nu, \infty]$ is the solar flux at wavenumber ν at the top of the atmosphere. Our model assumes a flat spectrum for the solar flux at the top of the atmosphere with $\pi F(\nu, \infty) = 5.0 \times 10^{13}$ photons cm^{-2} s^{-1}. The optical depth, τ, is

$$\tau(\nu, z) = \sec\theta \int_z n_{O_2}(z')\sum_j S_J(T)V(T, P, x, y)\,dz' \quad (4)$$

where θ is the solar zenith angle, and the integration is carried out from the altitude of interest, z, to the top of the atmosphere.

The sum inside the integral of equations (1) and (4) extends over all lines in the vibrational band, excluding the isotopic lines which are considered too weak to be significant. The following equation was used to calculate the line strengths at the temperature of interest

$$S_J(T) = \frac{S_J(T_s)Q_v(T_s)Q_R(T_s)}{Q_v(T)Q_R(T)} \times \exp\left(\frac{1.439\,E''(T - T_s)}{TT_S}\right), \quad (5)$$

where $S_J(T_s)$ = line strength at standard temperature (cm^{-1} mol^{-1} cm^{-2}), T_s = standard temperature (296 K), E'' = energy of the lower state in cm^{-1}, Q_v = vibrational partition function and Q_R = rotational partition function. The line strengths at standard temperature, $S_J(T_s)$, and the values for E'' were obtained from the AFCRL Atmospheric Line Parameters Compilation (McClatchey *et al.*, 1973). The ratio of the vibrational partition functions, $Q_v(T)/Q_v(T_s)$, is equal to 1.0 (McClatchey *et al.*, 1973). The rotational partition function at the temperature of interest was calculated using the equation

$$Q_R(T_s)/Q_R(T) = T_s/T. \quad (6)$$

The temperatures, pressures and densities as a function of altitude were obtained from a model atmosphere which incorporates data from three sources: the 1962 U.S. Standard Atmosphere (Kneizys *et al.*, 1980) for the lower atmosphere (0–52 km), profiles from Banks and Kocharts (1973) for the middle atmosphere (52–92 km), and the MSIS-83 (Hedin, 1983) model for the upper atmosphere (>92 km). The densities of ozone and atomic oxygen throughout the atmosphere were obtained from the Garcia–Solomon atmosphere model (S. Solomon, private communication, 1985).

The integration was performed with an altitude step size of 1 km from 0 to 40 km, and with a step size of 5 km from 40 to 120 km. For the integration over wavenumber a step size of 0.01 cm^{-1} was used throughout the band. Performing the integration with a step size of 0.001 cm^{-1} was found to make no significant difference in the results.

Figure 1 shows the calculated g factor versus altitude for the three main bands of the $O_2(^1\Sigma)$ system. The $A(0,0)$ band dominates the $B(1,0)$ and $\gamma(2,0)$ bands at all altitudes, so only the g factor for the A band is used in further calculations. Figure 2 shows the

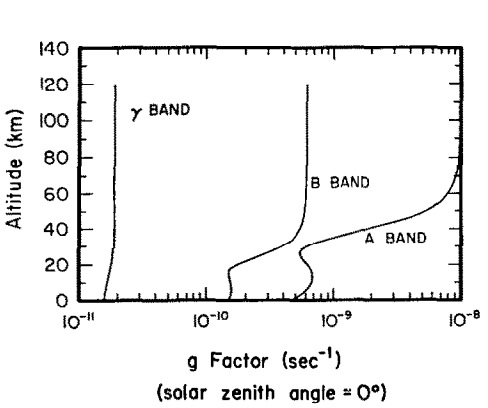

FIG. 1. CALCULATED g FACTOR VERSUS ALTITUDE FOR THE THREE MAIN BANDS OF THE $O_2(^1\Sigma)$ SYSTEM.

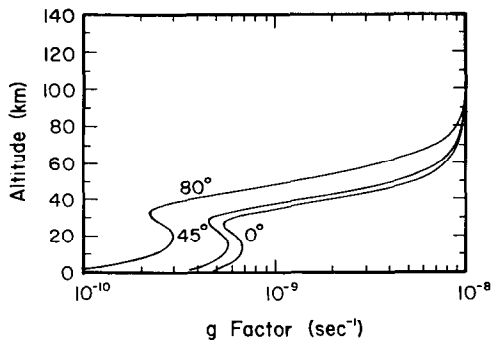

FIG. 2. THE A BAND g FACTOR AS A FUNCTION OF SOLAR ZENITH ANGLE.

change in the A band g factor for three different solar zenith angles of 0, 45 and 80°. As expected, the higher solar zenith angles cause a decline of the emission rate factor due to the increase in the attenuation of the solar flux as the path length is increased.

It can be seen in Figs 1 and 2 that the g factor steadily declines with decreasing altitude until approximately 30 km, at which point it begins to increase again. The cause of this increase in the g factor is the pressure broadening of the lines. While light at wavelengths near the center of the lines has become optically thick, the resonant scattering process is still significant in the wings of the broadened lines. If pressure broadening is excluded, the g factor decreases steadily with decreasing altitude, as can be seen in Fig. 3. It should be noted that the shape of the spectral lines in the wings is not well known and may not be well represented by a Voigt profile.

2.2. *Chemical production mechanisms.*

The chemistry of the O_2 atmospheric bands is reasonably simple. The Einstein A coefficient, $A_{1\Sigma}$, is approximately 0.085 s^{-1} (Burch and Gryvnak, 1969) implying that the lifetime of the $O_2(^1\Sigma)$ state is approximately 12 s. This lifetime is short enough so that transport can be ignored but long enough so that the state can be assumed to be in rotational equilibrium. Below we review the production of $O_2(^1\Sigma)$ due to quenching to $O(^1D)$ and the Barth type chemical process.

$O_2(b\,^1\Sigma_g^+)$ is formed by a quenching reaction with $O(^1D)$:

$$O(^1D)+O_2 \rightarrow O(^3P)+O_2(b\,^1\Sigma_g^+), \qquad (7)$$

with a reaction rate of $k_7 = 2.9\times 10^{-11}e^{67/T}\,cm^3\,s^{-1}$ (Streit *et al.*, 1976).

Below the lower thermosphere the main mechanisms for the production of $O(^1D)$ are the photodissociation of O_2 in the Schumann–Runge region and the dissociation of O_3:

$$O_2+h\nu(\lambda < 176\,nm) \rightarrow O(^1D)+O(^3P) \qquad (8)$$

$$O_3+h\nu(\lambda < 310\,nm) \rightarrow O(^1D)+O_2^*. \qquad (9)$$

Energetically, it is possible for ozone to dissociate directly into the $O_2(b\,^1\Sigma_g^+)$ state, but Gauthier and Snelling (1970, 1971) have shown this to be ineffective and it is not included here. The production of $O(^1D)$ by mechanisms (8) and (9) is found by integrating the dissociation cross section, σ, and the solar flux across wavenumber:

$$P[O(^1D)] = n_{O_2}(z)\int_\nu \pi F(\nu,z)\sigma_{O_2}(\nu)\,d\nu + n_{O_3}(z)\int_\nu \pi F(\nu,z)\sigma_{O_3}(\nu)\,d\nu. \qquad (10)$$

The solar flux, attenuated by O_2 and O_3, is given by

$$\pi F(\nu,z) = \pi F(\nu,\infty) \times \exp\left[-\left(\int_z \sigma_{O_2}(\nu)n_{O_2}(s)\,ds+\int_z \sigma_{O_3}(\nu)n_{O_3}(s)\,ds\right)\right], \qquad (11)$$

where the integral is along the line of sight from z towards the sun. The cross sections and solar flux were obtained from Olivero (1970).

Once produced, $O(^1D)$ can emit or be quenched by N_2 and O_2, so that its density at altitude z is given by

$$n_{O(^1D)}(z) = \frac{P[O(^1D)]}{A_{^1D}+k_{7a}n_{O_2}(z)+k_{^1D}n_{N_2}(z)}, \qquad (12)$$

with $k_{^1D} = 2.3\times 10^{-11}$ cm^3 s^{-1} and $A_{^1D} = 6.81\times 10^{-3}\,s^{-1}$. In our model $k_{7a} = k_7$, although these may be different. Since N_2 is the dominant quencher, the precise value of k_{7a} is not crucial. The production rate

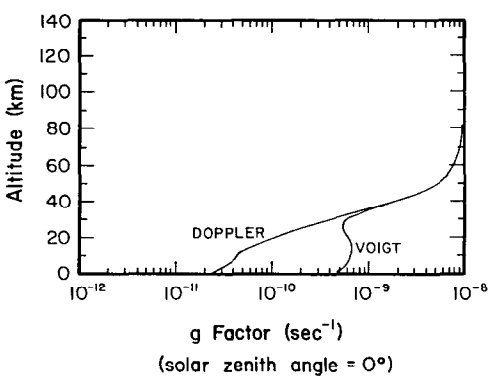

FIG. 3. COMPARISON OF THE A BAND g FACTOR USING A DOPPLER AND A VOIGT PROFILE.

of $O_2(^1\Sigma)$ due to $O(^1D)$ is then just

$$P_{O(^1D)}[O_2(^1\Sigma)] = k_7 n_{O_2}(z) n_{O(^1D)}(z). \quad (13)$$

The O_2 atmospheric band chemical source is provided in this model by a Barth type mechanism. Although the Chapman process cannot be ruled out, most evidence is consistent with the Barth reactions (Campbell and Gray, 1973; Greer *et al.*, 1981; Slanger and Black, 1977). Since we are looking at daytime emission, the chemical source is not a dominant process and knowledge of its exact nature is not critical. To obtain an approximate solution we chose to consider only the Barth process. The question is still not settled and as new information becomes available it will be incorporated into the model.

The Barth process contains two steps:

$$O + O + M \rightarrow O_2^* + M \quad (14)$$

with $k_{14} = 4.7 \times 10^{-33}(300/T)^2\alpha$ cm^6 s^{-1} (Campbell and Gray, 1973), followed by

$$O_2^* + O_2 \rightarrow O_2(^1\Sigma) + O_2 \quad (15)$$

with $k_{15} = 5.0 \times 10^{-13}\beta$ cm^{-1} s^{-1} (Greer *et al.*, 1981). The efficiency factor is $\alpha\beta = 0.80$. O_2^* can also be quenched by

$$O_2^* + O \rightarrow O_2 + O \quad (16)$$

with $k_{16} = 3 \times 10^{-11}$ cm^3 s^{-1} (Greer *et al.*, 1981), or emit with $A_{*O_2} = 0.002\,\text{s}^{-1}$ (Slanger, 1978). Here O_2^* is an excited O_2 molecule with a higher electronic state than $b\,^1\Sigma_g^+$. The production rate of $O_2(^1\Sigma)$ due to this Barth type chemical reaction is then given by

$$P_{\text{Barth}}[O_2(^1\Sigma)] = \frac{k_{15} n_{O_2}(z) k_{14} n_O(z)^2 n_M(z)}{A_{*O_2} + k_{15} n_{O_2}(z) + k_{16} n_O(z)} \quad (17)$$

2.3. *Loss processes*

The loss processes of the $O_2(^1\Sigma)$ state are emission and quenching by N_2 and O_2. The production mechanisms described above can produce $O_2(b\,^1\Sigma_g^+)$ molecules in the $v' = 0$, 1 or 2 levels. It is necessary, in principle, to consider emission and quenching from all three vibrational levels. In reality, the $v' = 1$ and $v' = 2$ states are rapidly deactivated to the $v' = 0$ level with rates of 2.2×10^{-11} cm^3 s^{-1} (Lee and Slanger, 1978) and 9×10^{-15} cm^3 s^{-1} (Schurath, 1975), respectively. This is much faster than the electronic quenching of molecules in the $v' = 0$ state to the $X\,^3\Sigma_g^-$ state, which is dominated by N_2 and goes at a rate of $k_{N2} = 2.2 \times 10^{-15}$ cm^3 s^{-1} (Martin *et al.*, 1976). Quenching by O_2 is much slower and has a rate of $k_{O_2} = 4 \times 10^{-17}$ cm^3 s^{-1} (Martin *et al.*, 1976). Consequently, it is reasonable to ignore emission from the higher vibrational levels and just consider that all production results in molecules in the $v' = 0$ level.

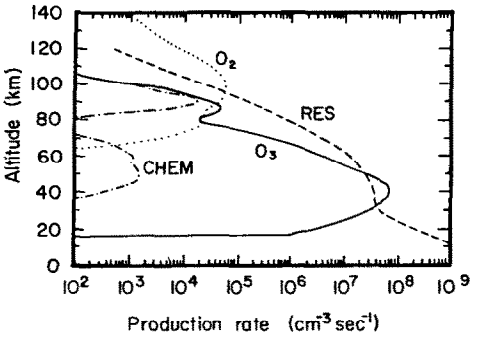

FIG. 4. PRODUCTION RATES OF $O_2(^1\Sigma)$.

3. DISCUSSION

The density of $O_2(b\,^1\Sigma_g^+)$ at some altitude z can now be written as

$$[O_2(b\,^1\Sigma_g^+)] = \frac{P_{\text{RES}} + P_{O(^1D)} + P_{\text{Barth}}}{A_{1\Sigma} + k_{N_2} n_{N_2}(z) + k_{O_2}(z)}. \quad (18)$$

Figure 4 shows the production rates of $O_2(^1\Sigma)$ due to each of the individual processes. The curve marked O_2 represents the production of $O_2(^1\Sigma)$ due to photodissociation of O_2 in the Schumann–Runge band followed by collisional energy transfer form $O(^1D)$. The curve marked O_3 represents the production of $O_2(^1\Sigma)$ due to photodissociation of O_3 followed by quenching of $O(^1D)$. The production of $O_2(^1\Sigma)$ due to resonant scattering in the A band is represented by the profile labeled RES, while the curve marked CHEM represents the production of $O_2(^1\Sigma)$ due to the Barth chemical process.

The following equation is used to calculate the volume emission rate in the $A(0,0)$ band

$$\eta_{O_2(^1\Sigma)}(z) = F_c A_{1\Sigma}[O_2(b\,^1\Sigma_g^+)], \quad (19)$$

where F_c is the Franck-Condon factor for the A band (0–0) and is equal to 0.93 (Nicholls, 1965). Figure 5

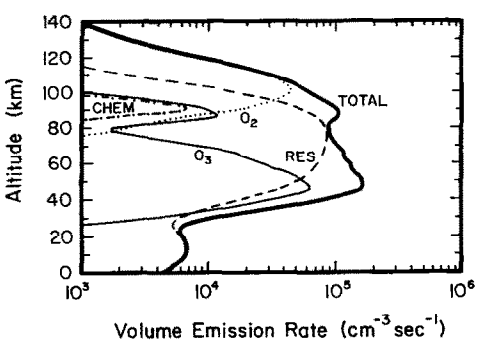

FIG. 5. VOLUME EMISSION RATES OF THE $O_2(^1\Sigma)$ A BAND.

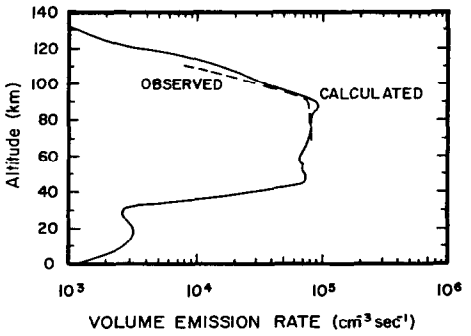

FIG. 6. COMPARISON OF CALCULATED TOTAL VOLUME EMISSION RATE AND OBSERVED VOLUME EMISSION RATE.

shows the volume emission rates of the $O_2(^1\Sigma)$ *A* band, labelled similarly to Fig. 4.

As a test of the validity of our calculations, the model was run under conditions similar to those of the actual observations of Wallace and Hunten (1968) (for 11 October 1966, latitude 32°, longitude 105°, local time of 4:22 pm and solar zenith angle of 75.5°). Figure 6 is a comparison of our total volume emission rate compared to the observational results of Wallace and Hunten (see Fig. 5 in Wallace and Hunten, 1968). Their data was only reliable in the 70–110 km altitude range and in this region our model is in excellent agreement with their observations. A slight discrepancy occurs near 90 km where the chemical source plays an important role, suggesting that the Barth reaction as incorporated here is still not the complete answer.

Acknowledgements—This work was supported by a grant from the National Aeronautics and Space Administration, grant number NAS 5-27751.

REFERENCES

Banks, P. M. and Kocharts, G. (1973) *Aeronomy*, parts A and B. Academic Press, New York.

Burch, D. E. and Gryvnak, D. A. (1969) Strengths, widths, and shapes of the oxygen lines near 13 100 cm^{-1} (7620 Å). *Appl. Opt.* **8**, 1493.

Campbell, I. M. and Gray, C. N. (1973) Rate constants for $O(^3P)$ recombination with $N(^4S)$. *Chem. Phys. Lett.* **18**, 607.

Drayson, S. R. (1976) Rapid computation of the Voigt profile. *J. quant. Spectrosc. radiat. Transfer* **16**, 611.

Gauthier, M. and Snelling, D. R. (1970) Formation of singlet molecular oxygen from the ozone photochemical system. *Chem. Phys. Lett.* **5**, 93.

Gauthier, M. and Snelling, D. R. (1971) Mechanism of singlet molecular oxygen formation from photolysis of ozone at 2537 Å. *Chem. Phys.* **54**, 4317.

Greer, R. G. H., Llewellyn, E. J., Solheim, B. H. and Witt, G. (1981) The excitation of $O_2(b\,^1\Sigma_g^+)$ in the nightglow. *Planet. Space Sci.* **29**, 383.

Hedin, A. E. (1983) A revised global thermospheric model based on mass spectrometer and incoherent scatter data MSIS:1983. *J. geophys. Res.* **88**, 10170.

Kneizys, F. X., Shettle, E. P., Gallery, W. O., Chetwynd, J. H. Jr., Abreu, L. W., Selby, J. E. A., Fenn, R. W. and McClatchey, R. A. (1980) *Atmospheric transmittance/radiance: computer code* LOWTRAN 5, *environmental research papers*, no. 687, AFGL-TR-80-0067. National Technical Information Service, Springfield, Virginia.

Lee, L. C. and Slanger, T. G. (1978) Observations on $O(^1D \rightarrow {}^3P)$ and $O_2(b\,^1\Sigma_g^+ \rightarrow X\,^3\Sigma_g^+)$ following O_2 photodissociation. *J. chem. Phys.* **69**, 4053.

Martin, L. R., Cohen, R. B. and Schatz, J. F. (1976) Quenching of laser induced fluorescence of $O_2(b\,^1\Sigma_g^+)$ by O_2 and N_2. *Chem. Phys. Lett.* **41**, 394.

McClatchey, R. A., Benedict, W. S., Clough, S. A., Burch, D. E., Calfee, R. F., Fox, K., Rothman, L. S. and Garing, J. S. (1973) *ARCRL atmospheric absorption line parameters compilation, environmental research papers*, No. 434, AFCRL-TR-73-0096. National Technical Information Service, Springfield, Virginia.

Nicholls, R. W. (1965) Franck–Condon factors to high vibrational quantum numbers V:O_2 band systems. *J. Res. NBS* **69A**, 369.

Olivero, J. J. (1970) Study of the Thermal Structure of the Mesosphere and Lower Thermosphere. Ph.D. Thesis (University of Michigan).

Schurath, U. (1975) The energy pooling reaction $2O_2(^1\Sigma_g) \rightarrow O_2(X\,^3\Sigma_g^-) + O_2(b\,^1\Sigma_g^+)$ formation, relaxation and quenching of vibrationally excited $O_2(b\,^1\Sigma_g^+)$. *J. Photochem.* **4**, 215.

Slanger, T. G. and Black, G. (1977) $O(^1S)$ in the lower thermosphere Chapman vs. Barth. *Planet. Space Sci.* **25**, 79.

Streit, G. E., Howard, C. J., Schmeltekopf, A. L., Davison, J. A. and Schiff, H. I. (1976) Temperature dependence of $O(^1D)$ rate constants for reactions with O_2, N_2, CO_2, O_3, and H_2O. *J. chem. Phys.* **65**, 4761.

Wallace, L. and Hunten, D. M. (1968) Dayglow of the Oxygen *A* Band. *J. geophys. Res.* **73**, 4813.